ETH
Eidgenössische Technische Hochschule Zürich
Swiss Federal Institute of Technology Zurich

Seminar for Applied Mathematics SAM

Entropy stable schemes on two-dimensional unstructured grids

D. Ray and P. Chandrashekar and U. Fjordholm and S. Mishra

Research Report No. 2014-28
October 2014

Seminar für Angewandte Mathematik
Eidgenössische Technische Hochschule
CH-8092 Zürich
Switzerland

Entropy stable schemes on two-dimensional unstructured grids

Deep Ray* Praveen Chandrashekar † Ulrik S. Fjordholm‡ Siddhartha Mishra §

Abstract

We propose an entropy stable high-resolution finite volume scheme to approximate systems of two-dimensional symmetrizable conservation laws on unstructured grids. The scheme is constructed using a judicious combination of entropy conservative fluxes and entropy-stable numerical dissipation operators. High resolution is achieved based on a piecewise linear reconstruction procedure satisfying a suitable sign property. The proposed scheme is demonstrated to robustly approximate complex flow features by a series of benchmark numerical experiments.

1 Introduction

Systems of conservation laws are encountered in numerous fields of science and engineering. Examples include the shallow water equations of oceanography, the Euler equations of aerodynamics and the MHD equations of plasma physics. In two space dimensions, a generic system of conservation laws is given by,

$$\begin{aligned} \partial_t \mathbf{U} + \partial_x \mathbf{f}_1(\mathbf{U}) + \partial_y \mathbf{f}_2(\mathbf{U}) = 0 \qquad & \forall\ \mathbf{x} = (x,y) \in \mathbb{R}^2,\ t \in \mathbb{R}^+ \\ \mathbf{U}(\mathbf{x},0) = \mathbf{U}_0(\mathbf{x}) \qquad & \forall\ \mathbf{x} \in \mathbb{R}^2. \end{aligned} \tag{1.1}$$

The vector of conserved variables is denoted by $\mathbf{U} : \mathbb{R}^2 \times \mathbb{R}^+ \to \mathbb{R}^n$, while $\mathbf{f}_1, \mathbf{f}_2$ are the Cartesian components of the flux vector. In particular, for the two-dimensional compressible Euler equations, we have

$$\mathbf{U} = \begin{pmatrix} \rho \\ \rho u \\ \rho v \\ E \end{pmatrix}, \qquad \mathbf{f}_1(\mathbf{U}) = \begin{pmatrix} \rho u \\ \rho u^2 + p \\ \rho uv \\ u(E+p) \end{pmatrix}, \qquad \mathbf{f}_2(\mathbf{U}) = \begin{pmatrix} \rho v \\ \rho uv \\ \rho v^2 + p \\ v(E+p) \end{pmatrix} \tag{1.2}$$

where ρ, $\mathbf{u} = (u,v)^\top$ and p denote the fluid density, velocity and pressure, respectively. The quantity E is the total energy per unit volume

$$E = \rho\left(\frac{1}{2}(u^2+v^2) + e\right), \tag{1.3}$$

where e is the specific internal energy given by a caloric equation of state, $e = e(\rho, p)$. The equation of state for ideal gas is given by

$$e = \frac{p}{(\gamma-1)\rho} \tag{1.4}$$

with $\gamma = c_p/c_v$ denoting the ratio of specific heats.

*TIFR Bangalore
†TIFR Bangalore
‡Department of Mathematical Sciences, Norwegian University of Science and Technology, Trondheim, N-7491, Norway
§Seminar for Applied Mathematics, ETH Zurich, Switzerland and Center of Mathematics for Applications, University of Oslo, Norway

It is well known that solutions to systems of conservation laws can develop discontinuities, such as shock waves and contact discontinuities, in finite time even when the initial data is smooth [5]. Hence, the solutions of systems of conservation laws are interpreted in a weak (distributional) sense. However, these weak solutions are not necessarily unique , and must be supplemented with additional conditions, known as the *entropy conditions*, in order to single out a physically relevant solution. Assume that for the system (1.1), there exists a convex function $\eta : \mathbb{R}^n \to \mathbb{R}$ and functions $q_i : \mathbb{R}^n \to \mathbb{R}, i = 1, 2$ such that

$$q_i'(\mathbf{U}) = \eta'(\mathbf{U})^\top \mathbf{f}_i'(\mathbf{U}) \qquad i = 1, 2. \tag{1.5}$$

The function η is known as an *entropy function*, while q_1, q_2 are the *entropy flux functions*. Additionally, $\mathbf{V} = \eta'(\mathbf{U})$ is called the (vector of) *entropy variables*. Multiplying (1.1) by $\mathbf{V}^\top$ results in the following additional conservation law for smooth solutions:

$$\partial_t \eta(\mathbf{U}) + \partial_x q_1(\mathbf{U}) + \partial_y q_2(\mathbf{U}) = 0. \tag{1.6}$$

The entropy condition states that weak solutions should satisfy the entropy inequality

$$\partial_t \eta(\mathbf{U}) + \partial_x q_1(\mathbf{U}) + \partial_y q_2(\mathbf{U}) \leqslant 0, \tag{1.7}$$

which is understood in the sense of distributions.

The convexity of $\eta(\mathbf{U})$ ensures the existence of a one-to-one mapping between $\mathbf{U}$ and $\mathbf{V}$, thus allowing the change of variables $\mathbf{U} = \mathbf{U}(\mathbf{V})$. The hyperbolic system (1.1) is *symmetrized* when written in terms of the entropy variables. In other words, for the transformed system

$$\partial_{\mathbf{V}} \mathbf{U} \partial_t \mathbf{V} + \partial_{\mathbf{V}} \mathbf{f}_1 \partial_x \mathbf{V} + \partial_{\mathbf{V}} \mathbf{f}_2 \partial_y \mathbf{V} = 0$$

the Jacobian $\partial_{\mathbf{V}} \mathbf{U}$ is symmetric positive definite, while $\partial_{\mathbf{V}} \mathbf{f}_1, \partial_{\mathbf{V}} \mathbf{f}_2$ are symmetric. In this direction, we have the important results due to Godunov [11] and Mock [22], which state that the hyperbolic system (1.1) is symmetrizable if and only if it is equipped with an entropy function $\eta(\mathbf{U})$ and corresponding entropy fluxes $q_1(\mathbf{U}), q_2(\mathbf{U})$.

Although no global existence and uniqueness results for entropy solutions of these systems are currently available, the entropy conditions do play an important role in providing global stability estimates. Formally integrating (1.7) in space and ignoring the boundary terms by assuming periodic or no-inflow boundary conditions, we get

$$\frac{\mathrm{d}}{\mathrm{d}t} \int_{\mathbb{R}^2} \eta(\mathbf{U}) \mathrm{d}\mathbf{x} \leqslant 0 \quad \Longrightarrow \quad \int_{\mathbb{R}^2} \eta(\mathbf{U}(\mathbf{x}, t)) \mathrm{d}\mathbf{x} \leqslant \int_{\mathbb{R}^2} \eta(\mathbf{U}_0(\mathbf{x})) \mathrm{d}\mathbf{x} \qquad \forall\ t > 0. \tag{1.8}$$

As η is convex, the above entropy bound gives rise to an a priori estimate on the solution of (1.1) in suitable L^p spaces [5].

Numerical methods for hyperbolic systems have undergone extensive development over the past few decades. Finite volume methods, in which the computational domain is divided into control volumes and a discrete version of the conservation law imposed on each control volume, are very popular. In particular, (approximate) Riemann solver based numerical flux functions, non-oscillatory reconstructions of the TVD, ENO, WENO type and strong stability preserving Runge-Kutta methods constitute an attractive and widely used package for the robust approximation of systems of conservation laws. An alternative is the use of Runge-Kutta Discontinuous Galerkin (DG) finite element methods [4] together with limiters to obtain non-oscillatory approximation.

Although many rigorous convergence results for these methods (at least for their first and second order versions) are known for *scalar conservation laws*, even in several space dimensions ([19, 18] and references therein), very few rigorous results are available for schemes approximating systems of conservation laws, particularly in several space dimensions. Since obtaining rigorous convergence results of

numerical approximation to entropy solutions seems out of reach currently, see [10] for a discussion on this issue, design of *entropy stable schemes* i.e, numerical schemes that satisfy a discrete form of the entropy inequality (1.7) is a reasonable goal. Note that entropy stable schemes automatically satisfy an L^p estimate and provide the only global stability estimates for numerical methods for multi-dimensional conservation laws.

The construction of entropy stable schemes for systems of conservation laws was pioneered by Tadmor in [27]. The construction is based on two ingredients – *(i)* construction of an entropy conservative flux satisfying a discrete entropy equality, and *(ii)* addition of suitable dissipation operators to satisfy a discrete entropy inequality. First-order entropy stable schemes, constructed by the procedure of Tadmor have been tested by Fjordholm et al. [7] for the shallow-water equations and Roe and Ismail [15] for the Euler equations and found to be efficient. Arbitrarily high-order entropy conservative fluxes for Cartesian grids were developed in [20]. However, the design of arbitrary-high order entropy stable schemes was only carried out recently by Fjordholm et al. in [8]. These so-called *TeCNO schemes* judiciously combine high-order entropy conservative fluxes with arbitrarily high-order numerical diffusion operators, based on piecewise polynomial reconstruction. The reconstructions have to satisfy the *sign property* at each interface to ensure entropy stability. It was shown in [9] that the standard ENO reconstruction procedure does satisfy the sign property. The resulting TeCNO schemes are only available for Cartesian (structured) grids in several space dimensions. However, many applications of interest, particularly in engineering, involve domains with complex geometry [6, 16], which can be more easily discretized using *unstructured grids*. First-order entropy-stable finite volume schemes for hyperbolic systems on unstructured meshes have been constructed in [21].

The aim of this paper is to propose an entropy-stable high-resolution finite volume scheme on unstructured grids in two space dimensions. Our construction involves the combination of entropy conservative fluxes, also considered in [21], together with a sign property preserving piecewise linear reconstruction. The rest of the paper is organized as follows. In Section 2 we describe the discretization of the domain and introduce the general semi-discrete scheme for system of conservation laws. Section 3 introduces the machinery for construction of entropy conservative and entropy stable schemes. Construction of higher order entropy stable schemes by the limited reconstruction of scaled entropy variables is also discussed. Several two-dimensional numerical results are presented in Section 4 to demonstrate the robustness of the proposed schemes. Concluding remarks are made in Section 5.

2 Discretization

The domain $\Omega \subset \mathbb{R}^2$ is discretized using triangles T with nodes denoted by $i, j, k, etc.$ For each edge of a triangle, we define the outward normal vectors with magnitude equal to the length of the corresponding edge. We use the notation $\mathbf{n}_i^T$ to describe the outward normal to the edge of T which is opposite to the vertex i. Furthermore, for each boundary edge e we denote the triangle adjacent to it by T_e and the outward normal to the edge e as $\mathbf{n}_e$. These are depicted in Figure 1.

Around each vertex i, the dual cell is constructed by joining the centroids of each adjoining triangle to the mid-points of its edges. This is known as the *median dual cell*. The *Voronoi dual cells* can also be generated in a similar manner by joining the mid-point of the triangle edges to the circumcenters instead of the centroids. The dual meshes are depicted in Figure 2. We adopt the *vertex-centered* approach for the finite volume schemes discussed below, where the dual cells are chosen as the control volumes and the solution (cell average) is stored at the nodes.

Using Gauss-Green's theorem for integration over a polygon, one can easily conclude that the sum of the outward normals of all the edges is zero. In particular, the outward normals of the triangle T sum to zero

$$\mathbf{n}_i^T + \mathbf{n}_j^T + \mathbf{n}_k^T = \mathbf{0}.$$

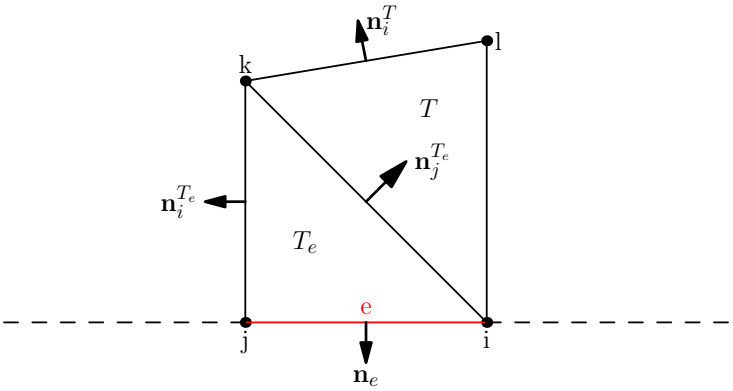

Figure 1: Triangle T and T_e with outward normals

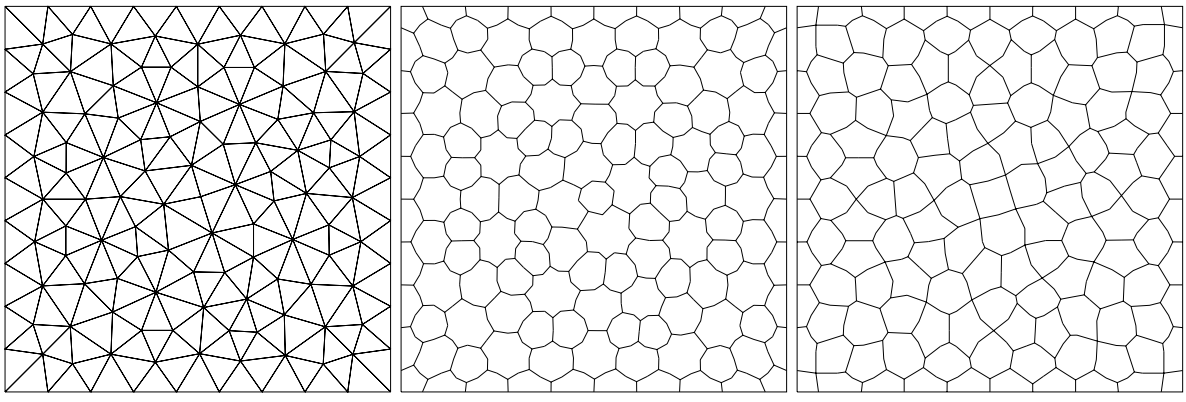

Figure 2: Mesh (a) primary; (b) median dual; Voronoi dual

Furthermore, we define

$$\mathbf{n}_{ij} = \int_{\partial C_i \cap \partial C_j} \tilde{\mathbf{n}} \mathrm{d}s,$$

where $\tilde{\mathbf{n}}$ is the unit normal vector to the faces of dual cell C_i common with the dual cell C_j. The quantity $\mathbf{n}_{ij}$ has units of length. The notation $j \in i$ will denote the set of vertices j neighbouring the vertex i, i.e., which are connected to vertex i through an edge.

The semi-discrete finite volume scheme corresponding to (1.1) is given by

$$\frac{\mathrm{d}\mathbf{U}_i}{\mathrm{d}t} + \frac{1}{|C_i|} \sum_{j \in i} \mathbf{F}_{ij} = 0 \tag{2.1}$$

where $\mathbf{U}_i$ is the cell average over the dual cell C_i and $\mathbf{F}_{ij} = \mathbf{F}(\mathbf{U}_i, \mathbf{U}_j, \mathbf{n}_{ij})$ is the numerical flux satisfying the following properties.

1. **Consistency:**
$$\mathbf{F}(\mathbf{U}, \mathbf{U}, \mathbf{n}) = \mathbf{f}(\mathbf{U}, \mathbf{n}) := \mathbf{f}_1(\mathbf{U}) n_1 + \mathbf{f}_2(\mathbf{U}) n_2 \qquad \forall\ \mathbf{U}, \mathbf{n}.$$

2. **Conservation:**
$$\mathbf{F}(\mathbf{U}_1, \mathbf{U}_2, \mathbf{n}) = -\mathbf{F}(\mathbf{U}_2, \mathbf{U}_1, -\mathbf{n}) \qquad \forall\ \mathbf{U}_1, \mathbf{U}_2, \mathbf{n}.$$

3 Entropy conservative and entropy stable schemes

As mentioned in the introduction, we aim to construct an entropy stable scheme to approximate (1.1). Following Tadmor [26] and a recent paper [21], the first step is the design of an entropy conservative scheme as outlined below.

3.1 Entropy conservative scheme

Definition 3.1. *The numerical scheme* (2.1) *is said to be* entropy conservative *if it satisfies the discrete entropy relation*

$$\frac{\mathrm{d}\eta(\mathbf{U}_i)}{\mathrm{d}t} + \frac{1}{|C_i|} \sum_{j \in i} q^*_{ij} = 0 \tag{3.1}$$

where q^*_{ij} is a consistent numerical entropy flux.

We introduce the following notation

$$\Delta(\cdot)_{ij} = (\cdot)_j - (\cdot)_i, \qquad \overline{(\cdot)}_{ij} = \frac{1}{2}\left((\cdot)_i + (\cdot)_j\right).$$

Moreover, we introduce the *entropy potential*

$$\psi(\mathbf{U}, \mathbf{n}) := \mathbf{V}(\mathbf{U})^\top \mathbf{F}(\mathbf{U}, \mathbf{n}) - q(\mathbf{U}, \mathbf{n})$$

where $q(\mathbf{U}, \mathbf{n}) := q_1(\mathbf{U}) n_1 + q_2(\mathbf{U}) n_2$. The next theorem gives a sufficient condition on the numerical flux which makes the scheme entropy conservative.

Theorem 3.2 (see [21])**.** *The numerical scheme* (2.1) *with the flux $\mathbf{F}^*$ is entropy conservative if*

$$\Delta \mathbf{V}_{ij}^\top \mathbf{F}^*_{ij} = \psi(\mathbf{U}_j, \mathbf{n}_{ij}) - \psi(\mathbf{U}_i, \mathbf{n}_{ij}). \tag{3.2}$$

Specifically, it satisfies (3.1) *with numerical entropy flux given by*

$$q^*_{ij} = q^*(\mathbf{U}_i, \mathbf{U}_j, \mathbf{n}_{ij}) = \overline{\mathbf{V}}_{ij}^\top \mathbf{F}^*_{ij} - \frac{1}{2}\left(\psi(\mathbf{U}_j, \mathbf{n}_{ij}) + \psi(\mathbf{U}_i, \mathbf{n}_{ij})\right).$$

Proof. Multiplying (2.1) by the entropy variables $\mathbf{V}_i$, we get

$$\begin{aligned}
\frac{\mathrm{d}}{\mathrm{d}t}\eta(\mathbf{U}_i) &= -\frac{1}{|C_i|}\sum_{j\in i}\mathbf{V}_i^\top \mathbf{F}_{ij}^* \\
&= -\frac{1}{|C_i|}\sum_{j\in i}\left(\overline{\mathbf{V}}_{ij} - \frac{1}{2}\Delta\mathbf{V}_{ij}\right)^\top \mathbf{F}_{ij}^* \\
&= -\frac{1}{|C_i|}\sum_{j\in i}\left(\overline{\mathbf{V}}_{ij}\mathbf{F}_{ij}^* - \frac{1}{2}\left(\psi(\mathbf{U}_j,\mathbf{n}_{ij}) - \psi(\mathbf{U}_i,\mathbf{n}_{ij})\right)\right) \\
&= -\frac{1}{|C_i|}\sum_{j\in i}\left(\overline{\mathbf{V}}_{ij}\mathbf{F}_{ij}^* - \frac{1}{2}\left(\psi(\mathbf{U}_j,\mathbf{n}_{ij}) + \psi(\mathbf{U}_i,\mathbf{n}_{ij})\right)\right) - \frac{1}{|C_i|}\sum_{j\in i}\psi(\mathbf{U}_i,\mathbf{n}_{ij}) \\
&= -\frac{1}{|C_i|}\sum_{j\in i} q_{ij}^*
\end{aligned}$$

where we have used the fact that $\sum_{j\in i}\psi(\mathbf{U}_i,\mathbf{n}_{ij}) = 0$ since $\sum_{j\in i}\mathbf{n}_{ij} = 0$. □ □

Harten [13] has shown that the Euler equations are equipped with a family of entropy pairs of the form

$$\eta(\mathbf{U}) = -\frac{\rho h(s)}{\gamma - 1}, \quad q_1(\mathbf{U}) = -\frac{\rho u h(s)}{\gamma - 1}, \quad q_2(\mathbf{U}) = -\frac{\rho v h(s)}{\gamma - 1}$$

with an additional constraint $h''/h' < \gamma^{-1}$ to enforce convexity of η. Here $s = \ln(p) - \gamma\ln(\rho)$ is the non-dimensional specific entropy. Hughes et al.[14] have shown that this form of entropy pairs can be extended to the Navier-Stokes equations, where the symmetrization of the heat conduction term puts the restriction that $h(s)$ can be atmost affine. A convenient choice which we shall adhere to for the rest of this paper is

$$\eta(\mathbf{U}) = -\frac{\rho s}{\gamma - 1}, \quad q_1(\mathbf{U}) = -\frac{\rho u s}{\gamma - 1}, \quad q_2(\mathbf{U}) = -\frac{\rho v s}{\gamma - 1}. \tag{3.3}$$

The corresponding entropy variables $\mathbf{V}$ are given by

$$\mathbf{V} = \begin{pmatrix} \frac{\gamma - s}{\gamma - 1} - \beta|\mathbf{u}|^2 \\ 2\beta\mathbf{u} \\ -2\beta \end{pmatrix} \tag{3.4}$$

where $\beta = \rho/(2p)$. Next, we briefly describe two important examples of entropy conservative fluxes which have been designed for the Euler equations.

Example 3.3. Roe and Ismail [15] have constructed a numerical flux for the Euler equations satisfying (3.2). They introduce the parameter vector

$$\mathbf{Z} = \begin{pmatrix} Z_1 \\ Z_2 \\ Z_3 \\ Z_4 \end{pmatrix} = \sqrt{\frac{\rho}{p}}\begin{pmatrix} 1 \\ u \\ v \\ p \end{pmatrix}$$

and write the entropy conservative flux in terms of $\mathbf{Z}$ as follows.

$$\mathbf{F}^*_{ij} = \begin{pmatrix} F^{*,\rho} \\ F^{*,m1} \\ F^{*,m2} \\ F^{*,e} \end{pmatrix} = \begin{pmatrix} \overline{Z}_n \widehat{Z}_4 \\ \frac{\overline{Z}_4}{\overline{Z}_1} n_1 + \frac{\overline{Z}_2}{\overline{Z}_1} F^{*,\rho} \\ \frac{\overline{Z}_4}{\overline{Z}_1} n_2 + \frac{\overline{Z}_3}{\overline{Z}_1} F^{*,\rho} \\ F^{*,e} \end{pmatrix}$$

$$F^{*,e} = \frac{1}{2\overline{Z}_1} \left[\frac{(\gamma+1)}{(\gamma-1)} F^{*,\rho} + \overline{Z}_2 F^{*,m1} + \overline{Z}_3 F^{*,m2} \right]$$

where

$$\overline{Z}_n = \overline{Z}_2 n_1 + \overline{Z}_3 n_2$$

and $\widehat{\phi}_{ij} = \frac{\phi_j - \phi_i}{\ln(\phi_j) - \ln(\phi_i)}$ is the logarithmic average which is well defined for strictly positive quantities ϕ.

Example 3.4. An entropy conservative flux for the Euler equations, which also preserves kinetic energy was introduced in [3]

$$\mathbf{F}^* = \begin{pmatrix} F^{*,\rho} \\ F^{*,m1} \\ F^{*,m2} \\ F^{*,e} \end{pmatrix} = \begin{pmatrix} \widehat{\rho}\overline{u}_n \\ \tilde{p} n_1 + \overline{u} F^{*,\rho} \\ \tilde{p} n_2 + \overline{v} F^{*,\rho} \\ F^{*,e} \end{pmatrix}, \qquad F^{*,e} = \left[\frac{1}{2(\gamma-1)\widehat{\beta}} - \frac{1}{2}\overline{|\mathbf{u}|^2} \right] F^{*,\rho} + \overline{\mathbf{u}} \cdot \mathbf{F}^{*,m}$$

where

$$\overline{u}_n = \overline{u} n_1 + \overline{v} n_2, \qquad \tilde{p} = \frac{\overline{\rho}}{2\overline{\beta}}.$$

and $\widehat{\rho}, \widehat{\beta}$ are the logarithmic averages of the respective quantities. The crucial property for kinetic energy preservation as given by Jameson [17], is that the momentum flux should be of the form $\mathbf{F}^m = p\mathbf{n} + \overline{\mathbf{u}} F^\rho$ for any consistent approximations for p and F^ρ.

3.2 First order entropy stable scheme

The entropy of hyperbolic conservation laws is conserved only if the solution is smooth. However, entropy is dissipated near discontinuities like shocks, in accordance to the entropy condition (1.7). It is well known [27] that an entropy conservative scheme, although suitable for smooth solutions, can be very oscillatory at shocks. Hence, we need to introduce additional dissipation terms to construct entropy stable schemes.

Definition 3.5. *The numerical scheme* (2.1) *is said to be* entropy stable *if it satisfies the discrete entropy relation*

$$\frac{d\eta(\mathbf{U}_i)}{dt} + \frac{1}{|C_i|} \sum_{j \in i} q_{ij} \leqslant 0 \tag{3.5}$$

where q_{ij} is a consistent numerical entropy flux.

To dissipate entropy we follow [27, 8] and add entropy variable-based numerical dissipation to the entropy conservative numerical flux $\mathbf{F}^*_{ij}$ in the form

$$\mathbf{F}_{ij} = \mathbf{F}^*_{ij} - \frac{1}{2}\mathbf{D}_{ij}\Delta\mathbf{V}_{ij} \tag{3.6}$$

for a symmetric positive semi-definite matrix $\mathbf{D}_{ij}$, i.e., $\mathbf{D}_{ij} = \mathbf{D}_{ij}^\top \geqslant 0$. The diffusion matrix must also satisfy $\mathbf{D}_{ij} = \mathbf{D}_{ji}$ to ensure that the numerical flux is conservative.

Lemma 3.6. *The semi-discrete numerical scheme* (2.1) *with numerical flux given by* (3.6) *is entropy stable; specifically, it satisfies the discrete entropy inequality* (3.5) *with numerical entropy flux given by*

$$q_{ij} = q^*_{ij} - \frac{1}{2}\overline{\mathbf{V}}^\top_{ij}\mathbf{D}_{ij}\Delta\mathbf{V}_{ij}.$$

Proof. Multiplying (2.1) by $\mathbf{V}_i$ and following the algebraic manipulations similar to those in Theorem 3.2, we get

$$\begin{aligned}
\frac{\mathrm{d}}{\mathrm{d}t}\eta(\mathbf{U}_i) &= -\frac{1}{|C_i|}\sum_{j\in i}\mathbf{V}_i^\top\mathbf{F}_{ij} \\
&= -\frac{1}{|C_i|}\sum_{j\in i}\left[q^*_{ij} - \frac{1}{2}\left(\overline{\mathbf{V}}_{ij} - \frac{1}{2}\Delta\mathbf{V}_{ij}\right)^\top\mathbf{D}_{ij}\Delta\mathbf{V}_{ij}\right] \\
&= -\frac{1}{|C_i|}\sum_{j\in i}q_{ij} - \frac{1}{4|C_i|}\sum_{j\in i}\Delta\mathbf{V}_{ij}^\top\mathbf{D}_{ij}\Delta\mathbf{V}_{ij} \\
&\leqslant -\frac{1}{|C_i|}\sum_{j\in i}q_{ij}
\end{aligned}$$

since $\Delta\mathbf{V}_{ij}^\top\mathbf{D}_{ij}\Delta\mathbf{V}_{ij} \geqslant 0$. Moreover it is easy to see that q_{ij} as defined in the theorem is a consistent numerical entropy flux. □ □

3.3 Dissipation operator

In general, any symmetric positive semi-definite matrix $\mathbf{D}_{ij}$ can be chosen as the dissipation operator. However, we shall make a specific choice by referring to Roe's approximate Riemann solver [25], which is based on the linearization of the nonlinear conservation law about some average state. The numerical flux of the Roe scheme has the form

$$\mathbf{F}_{ij} = \frac{1}{2}\left(\mathbf{f}(\mathbf{U}_i, \mathbf{n}_{ij}) + \mathbf{f}(\mathbf{U}_j, \mathbf{n}_{ij})\right) - \frac{1}{2}\mathbf{R}_{ij}\mathbf{\Lambda}_{ij}\mathbf{R}_{ij}^{-1}\Delta\mathbf{U}_{ij} \tag{3.7}$$

where $\mathbf{R}$ is the matrix of eigenvectors of the flux Jacobian $\partial_{\mathbf{U}}\mathbf{f}(\mathbf{U}, \mathbf{n})$ and $\mathbf{\Lambda}$ is the non-negative diagonal matrix

$$\mathbf{\Lambda} = \mathrm{diag}\Big(|\lambda_1|, \ldots, |\lambda_n|\Big)$$

with λ_k being the eigenvalues of the flux Jacobian. These matrices are evaluated at the Roe average state.

The dissipation in (3.7) can be written in terms of the jump in the entropy variables, by linearizing the jump in the conserved variables as $\Delta\mathbf{U} = \partial_{\mathbf{V}}\mathbf{U}\Delta\mathbf{V}$, where the Jacobian $\partial_{\mathbf{V}}\mathbf{U}$ is symmetric positive definite [27]. The eigenvector rescaling theorem of Barth [1] ensures the existence of a scaling of the eigenvectors $\mathbf{R} \to \widetilde{\mathbf{R}}$, such that $\partial_{\mathbf{V}}\mathbf{U} = \widetilde{\mathbf{R}}\widetilde{\mathbf{R}}^\top$. The Roe-type flux can thus be re-written as

$$\mathbf{F}_{ij} = \frac{1}{2}\left(\mathbf{f}(\mathbf{U}_i, \mathbf{n}_{ij}) + \mathbf{f}(\mathbf{U}_j, \mathbf{n}_{ij})\right) - \frac{1}{2}\widetilde{\mathbf{R}}_{ij}\mathbf{\Lambda}_{ij}\widetilde{\mathbf{R}}_{ij}^\top\Delta\mathbf{V}_{ij}.$$

This motivates us to choose the *Roe-type* dissipation operator

$$\mathbf{D}_{ij} = \widetilde{\mathbf{R}}_{ij}\mathbf{\Lambda}_{ij}\widetilde{\mathbf{R}}_{ij}^\top \tag{3.8}$$

which is clearly symmetric positive semi-definite. For convenience we will drop the $\widetilde{(.)}$ notation for the remainder of this paper, where it will be understood that $\mathbf{R}_{ij}$ denotes the scaled eigenvectors. The

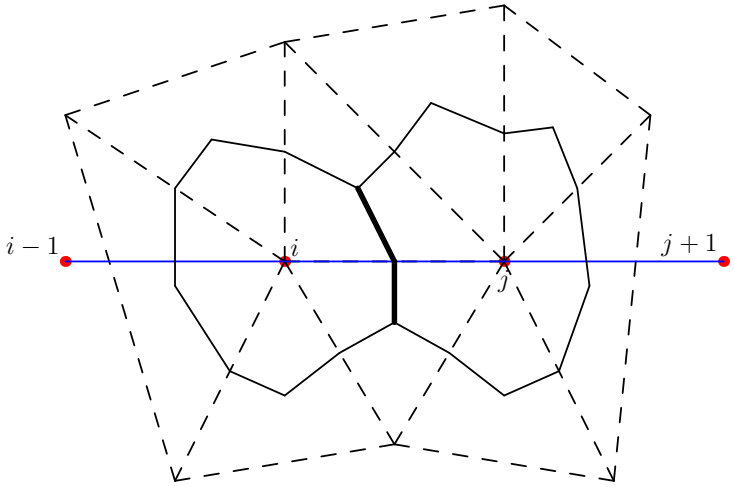

Figure 3: Stencil for reconstruction

matrices are evaluated at some average state depending on $\mathbf{U}_i$ and $\mathbf{U}_j$. To ensure that $\mathbf{F}_{ij}$ is conservative we require that $\mathbf{R}_{ij} = -\mathbf{R}_{ji}$. The specific form of the matrices chosen for the Euler equations are described in Appendix A.

Remark 3.7. *The Roe type dissipation operator, as chosen above, is just one of a whole host of alternatives when it comes to the choice of numerical dissipation operators [8]. In particular, we can choose* $\mathbf{\Lambda} = \max_i |\lambda_i| \mathbf{I}$ *to obtain a Rusanov type dissipation operator. Further examples of polynomial viscosity operators are provided in [8].*

3.4 High-order diffusion operators

For smooth solutions $\Delta \mathbf{V}_{ij} = \mathcal{O}(|\Delta \mathbf{x}_{ij}|)$ so that the diffusion term in schemes of the form (3.6) is just first order accurate. The first order scheme is a consequence of taking the solution to be constant in each cell and equal to the cell average value. In order to obtain a higher order scheme, we need to appropriately reconstruct the solution to the cell interfaces. Consider the cell interface between two control volumes C_i and C_j, as shown in Figure 3. In order to reconstruct the variables from each cell, we require additional nodes which we refer to as *phantom nodes*. These can be chosen by extending the line joining vertices i and j on both sides by a distance equal to the distance between the two nodes.

Corresponding to this particular cell interface, let $\mathbf{V}_i(\mathbf{x})$ and $\mathbf{V}_j(\mathbf{x})$ be polynomial reconstructions of the entropy variable in C_i and C_j respectively. We denote the reconstructed values at the cell interface, and the difference between them by

$$\mathbf{V}_{ij} = \mathbf{V}_i(\mathbf{x}_{ij}), \qquad \mathbf{V}_{ji} = \mathbf{V}_j(\mathbf{x}_{ij}), \qquad [\![\mathbf{V}]\!]_{ij} = \mathbf{V}_{ji} - \mathbf{V}_{ij} \tag{3.9}$$

where $\mathbf{x}_{ij}$ is the position vector of the the mid-point between vertices i and j. In order to get a second order dissipation operator, the polynomial reconstruction in each cell must be at least linear. The following result ensures that the reconstruction does not destroy entropy stability.

Lemma 3.8 (see [8])**.** *For each pair* (i, j)*, let* $\mathbf{R}_{ij}$ *be non-singular, let* $\mathbf{\Lambda}_{ij}$ *be any non-negative diagonal matrix, and define the numerical diffusion matrix*

$$\mathbf{D}_{ij} = \mathbf{R}_{ij} \mathbf{\Lambda}_{ij} \mathbf{R}_{ij}^\top.$$

Let $\mathbf{V}_i(x)$ and $\mathbf{V}_j(x)$ be polynomial reconstructions of the entropy variables in C_i and C_j respectively such that there exists a diagonal matrix $\mathbf{B}_{ij} \geqslant 0$ such that

$$[\![\mathbf{V}]\!]_{ij} = \left(\mathbf{R}_{ij}^\top\right)^{-1} \mathbf{B}_{ij} \mathbf{R}_{ij}^\top \Delta \mathbf{V}_{ij}. \tag{3.10}$$

Then the scheme with the numerical flux

$$\mathbf{F}_{ij} = \mathbf{F}_{ij}^* - \frac{1}{2} \mathbf{D}_{ij} [\![\mathbf{V}]\!]_{ij} \tag{3.11}$$

is entropy stable with numerical entropy flux

$$q_{ij} := q_{ij}^* - \frac{1}{2} \overline{\mathbf{V}}_{ij}^\top \mathbf{D}_{ij} [\![\mathbf{V}]\!]_{ij}.$$

Proof. As in the proof of Lemma 3.6, consider (2.1) with the flux defined by (3.11) and multiply it by the entropy variables $\mathbf{V}_i$ to get

$$\begin{aligned}
\frac{\mathrm{d}}{\mathrm{d}t} \eta(\mathbf{U}_i) &= -\frac{1}{|C_i|} \sum_{j \in i} \mathbf{V}_i^\top \mathbf{F}_{ij} \\
&= -\frac{1}{|C_i|} \sum_{j \in i} q_{ij}^* + \frac{1}{2|C_i|} \sum_{j \in \mathcal{N}_i} \left[\left(\overline{\mathbf{V}}_{ij} - \frac{1}{2} \Delta \mathbf{V}_{ij} \right)^\top \mathbf{D}_{ij} [\![\mathbf{V}]\!]_{ij} \right] \\
&= -\frac{1}{|C_i|} \sum_{j \in i} \left[q_{ij}^* - \frac{1}{2} \overline{\mathbf{V}}_{ij}^\top \mathbf{D}_{ij} [\![\mathbf{V}]\!]_{ij} \right] - \frac{1}{4|C_i|} \sum_{j \in i} \Delta \mathbf{V}_{ij}^\top \mathbf{R}_{ij} \mathbf{\Lambda}_{ij} \mathbf{B}_{ij} \mathbf{R}_{ij}^\top \Delta \mathbf{V}_{ij}.
\end{aligned}$$

Since $\mathbf{R}_{ij} \mathbf{\Lambda}_{ij} \mathbf{B}_{ij} \mathbf{R}_{ij}^\top$ is symmetric positive semi-definite, we get

$$\frac{\mathrm{d}}{\mathrm{d}t} \eta(\mathbf{U}_i) + \frac{1}{|C_i|} \sum_{j \in i} q_{ij} \leqslant 0.$$

□ □

3.4.1 Reconstruction procedure

In order to use Lemma 3.8, we describe a reconstruction procedure that satisfies (3.10). For each cell interface described by the neighbouring vertices i and j, define the *scaled entropy variables* $\mathbf{Z} = \mathbf{R}_{ij}^\top \mathbf{V}$. Given the entropy variables $\{\mathbf{V}_i\}_i$, we reconstruct in the scaled entropy variables $\{\mathbf{Z}_i\}_i$ to obtain the reconstructed states $\mathbf{Z}_{ij} = \mathbf{Z}_i(x_{ij})$ and $\mathbf{Z}_{ji} = \mathbf{Z}_j(x_{ij})$. We choose the corresponding reconstructed states for the entropy variables as

$$\mathbf{V}_{ij} = (\mathbf{R}_{ij}^\top)^{-1} \mathbf{Z}_{ij}, \qquad \mathbf{V}_{ji} = (\mathbf{R}_{ij}^\top)^{-1} \mathbf{Z}_{ji}$$

Thus, the dissipation terms in the flux given by (3.11) can be written in terms of the scaled entropy variables as

$$\mathbf{D}_{ij} [\![\mathbf{V}]\!]_{ij} = \mathbf{R}_{ij} \mathbf{\Lambda}_{ij} [\![\mathbf{Z}]\!]_{ij}$$

The condition given by (3.10) can now be interpreted in terms of the scaled variables as

$$[\![\mathbf{Z}]\!]_{ij} = \mathbf{B}_{ij} \Delta \mathbf{Z}_{ij}$$

for some diagonal matrix $\mathbf{B}_{ij}$ with non-negative entries. Componentwise, this further reduces to a *sign property* on the n different components Z of $\mathbf{Z}$:

$$\operatorname{sign}\Big([\![Z]\!]_{ij} \Big) = \operatorname{sign}\Big(\Delta Z_{ij} \Big). \tag{3.12}$$

3.4.2 Second order reconstruction

We now describe a reconstruction procedure of scaled entropy variables appearing in the dissipation terms, which satisfies the sign property. In practice we never construct the polynomials $\mathbf{V}_i(x)$ but we directly approximate the interface value of scaled entropy variables. Consider the stencil shown in Figure 3. The scaled entropy variables with respect to the interface between nodes i and j are given by

$$\mathbf{Z}_i = \mathbf{R}_{ij}^\top \mathbf{V}_i, \qquad \mathbf{Z}_j = \mathbf{R}_{ij}^\top \mathbf{V}_j \tag{3.13}$$

Assume that the gradients of $\mathbf{Z}$ are available at the vertices and define the following differences.

- The forward differences

$$\Delta_{ij}^f = \Delta Z_{ij}, \qquad \Delta_{ji}^f = Z_{j+1} - Z_j = 2\nabla_h Z_j \cdot (\mathbf{x}_j - \mathbf{x}_i) - \Delta Z_{ij} \tag{3.14}$$

- The backward differences

$$\Delta_{ij}^b = Z_i - Z_{i-1} = 2\nabla_h Z_i \cdot (\mathbf{x}_j - \mathbf{x}_i) - \Delta Z_{ij}, \qquad \Delta_{ji}^b = \Delta Z_{ij}. \tag{3.15}$$

The reconstructed values of $\mathbf{Z}$ at the interface are given by

$$Z_{ij} = Z_i + \frac{1}{2}\mathcal{M}\left(\Delta_{ij}^f, \Delta_{ij}^b\right), \qquad Z_{ji} = Z_j - \frac{1}{2}\mathcal{M}\left(\Delta_{ji}^f, \Delta_{ji}^b\right) \tag{3.16}$$

for each component Z of $\mathbf{Z}$, where we have used the minmod slope limiter function

$$\mathcal{M}(a,b) = \begin{cases} s\min(|a|,|b|) & \text{if} \quad s := \operatorname{sign}(a) = \operatorname{sign}(b) \\ 0 & \text{otherwise.} \end{cases}$$

Lemma 3.9. *The reconstruction of the scaled entropy variables described by* (3.16)*,* (3.14) *and* (3.15) *satisfies the sign property* (3.12)*.*

Proof. Consider

$$Z_{ji} - Z_{ij} = (Z_j - Z_i) - \frac{1}{2}\left[\mathcal{M}\left(\Delta_{ji}^f, \Delta_{ji}^b\right) + \mathcal{M}\left(\Delta_{ij}^f, \Delta_{ij}^b\right)\right].$$

If $Z_j - Z_i \geqslant 0$, then

$$\mathcal{M}\left(\Delta_{ij}^f, \Delta_{ij}^b\right) \leqslant \Delta_{ij}^f, \qquad \mathcal{M}\left(\Delta_{ji}^f, \Delta_{ji}^b\right) \leqslant \Delta_{ji}^b = \Delta_{ij}^f.$$

Thus,

$$Z_{ji} - Z_{ij} \geqslant (Z_j - Z_i) - \frac{1}{2}\left[2\Delta_{ij}^f\right] = 0.$$

Similarly, if $Z_j - Z_i \leqslant 0$, then

$$\mathcal{M}\left(\Delta_{ij}^f, \Delta_{ij}^b\right) \geqslant \Delta_{ij}^f, \qquad \mathcal{M}\left(\Delta_{ji}^f, \Delta_{ji}^b\right) \geqslant \Delta_{ji}^b = \Delta_{ij}^f$$

giving us

$$Z_{ji} - Z_{ij} \leqslant (Z_j - Z_i) - \frac{1}{2}\left[2\Delta_{ij}^f\right] = 0.$$

Hence, the reconstruction satisfies the sign property. □ □

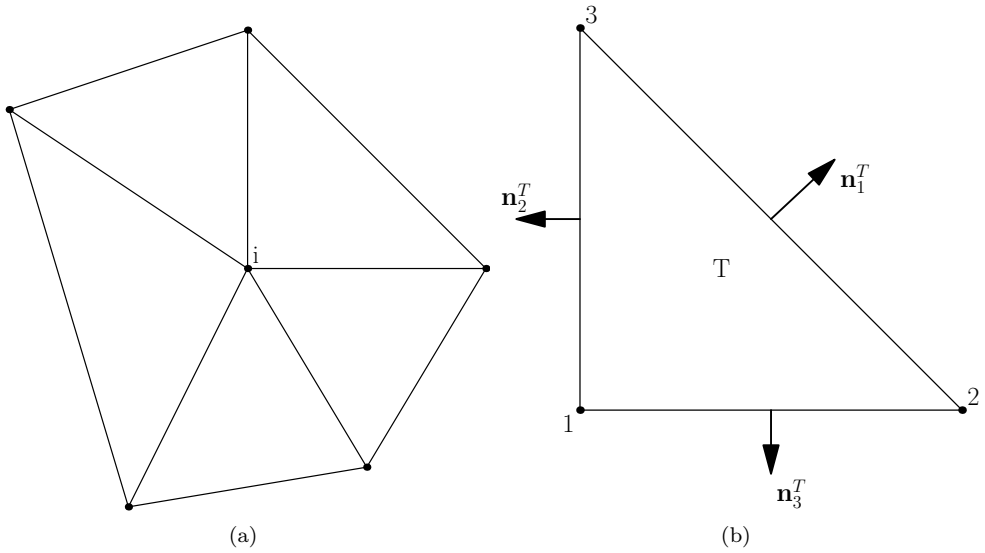

Figure 4: (a) Stencil for gradient evaluation at node i, (b) neighbouring triangle T

3.4.3 Computation of gradients

The second-order limited reconstruction described above requires the evaluation of nodal gradients of scaled entropy variables. We evaluate these gradient as

$$\nabla_h \mathbf{Z}_i = \mathbf{R}_{ij}^\top \nabla_h \mathbf{V}_i$$

where $\nabla_h \mathbf{V}_i$ must be numerically approximated. Consider the node i and the set of neighbouring primary triangular cells denoted by $T \in i$, as shown in Figure 4. The cell-gradients on each neighbouring triangle T is approximated by

$$\nabla_h \mathbf{V}^T = -\frac{1}{2|T|}\left(\mathbf{V}_1 \otimes \mathbf{n}_1^T + \mathbf{V}_2 \otimes \mathbf{n}_2^T + \mathbf{V}_3 \otimes \mathbf{n}_3^T\right) \tag{3.17}$$

where $\mathbf{X} \otimes \mathbf{Y} = \left(\mathbf{X}_m \mathbf{Y}_n\right)_{m,n}$ denotes the outer product. This approximation is exact for affine functions, and thus second order accurate. Finally, the gradient at node i is approximated as

$$\nabla_h \mathbf{V}_i = \frac{\sum\limits_{T \in i} |T| \nabla_h \mathbf{V}^T}{\sum\limits_{T \in i} |T|}. \tag{3.18}$$

4 Numerical results

We now present the numerical results of the scheme discussed above on several standard two dimensional test cases. We introduce the following nomenclature for various schemes that are tested in this section. The kinetic energy preserving and entropy conservative scheme from Example 3.4 will be referred to as the KEPEC scheme. The KEPEC scheme with the first order entropy variable based dissipation operator is termed as the KEPES scheme. The second order limited reconstruction of the scaled entropy variables

with the KEPES scheme will be referred to as the KEPES-TeCNO scheme. The KEPES scheme with a pure second order reconstruction of the scaled entropy variables using central undivided differences

$$Z_{ij} = Z_i + \frac{1}{2}\left(\frac{\Delta_{ij}^f + \Delta_{ij}^b}{2}\right), \qquad Z_{ji} = Z_j - \frac{1}{2}\left(\frac{\Delta_{ji}^f + \Delta_{ji}^b}{2}\right)$$

will be called KEPES2. Note that this scheme is not necessarily entropy stable as this unlimited reconstruction need not satisfy the sign property. The original Roe scheme [25] is used for comparison of numerical results.

The semi-discrete scheme is integrated in time using the explicit Strong Stability Preserving Runge-Kutta 3-stage scheme (SSP-RK3) method [12]. The Lower-Upper Symmetric Gauss Seidel method (LU-SGS) [2] is used for implicit time integration, and is preferred for steady problems as it allows larger time steps. In all test cases we consider the ideal gas with $\gamma = 1.4$ except when indicated otherwise.

4.1 Modified shock tube problem

This test case describes a one-dimensional shock tube problem of the Sod type. The primary and the Voronoi dual meshes used for the simulations are shown in Figure 5. We consider a rectangular domain $[0, 1] \times [0, 0.4]$ and discretize it with 100 nodes in the direction of the flow, and 80 nodes along the flow cross-section. The left state is given by $(\rho_L, u_L, v_L, p_L) = (1.0, 0.75, 0.0, 1.0)$ and the right state is given by $(\rho_R, u_R, v_R, p_R) = (0.125, 0.0, 0.0, 0.1)$, with the initial discontinuity along $x = 0.3$. Time integration is performed using SSP-RK3 with CFL=0.3.

The Roe scheme gives an entropy violating jump in the expansion region where the flow becomes sonic, as shown in Figure 6. This is not surprising as we have not added any entropy fix to the standard Roe scheme [25]. However, both the KEPES and KEPES-TeCNO schemes, being entropy stable, do not suffer from this problem. The comparison in Figure 7 shows that the high-resolution KEPES-TeCNO scheme is significantly more accurate as compared to KEPES. Convergence is demonstrated in Figure 8, where the solutions are evaluated using KEPES-TeCNO on three levels of uniform grid refinements, with the number of vertices along the streamwise direction being $N = 100, 200$ and 400 respectively.

4.2 Supersonic flow over wedge

This test case involves a weak oblique shock which occurs when a supersonic flow is 'turned into itself' due to the presence of a wedge. The wedge is inclined at an angle of 10 degrees to the horizontal. The farfield Mach number is 2, with slip boundary conditions on the wedge. The mesh has 18848 nodes and we use median dual cells as control volumes. Time integration is performed using LU-SGS. As can be seen in Figure 9, the shock profile is quite dissipated with KEPES. But, the minmod reconstruction in KEPES-TeCNO scheme leads to a much sharper shock profile, that is comparable to the one computed by the Roe scheme with MUSCL type reconstruction and van Albada limiter.

4.3 Transonic flow past NACA-0012 airfoil

This is an example of a symmetric NACA-0012 airfoil placed in a freestream Mach number of 0.85 and angle of attack of 2 degrees. The flow develops shocks both on the upper and lower airfoil surfaces. We compute this flow on a triangular grid by considering the median dual cells, containing 180 points on the airfoil surface and 20 points on the farfield boundary which is a circle, with a total of 6402 vertices. Time integration is performed using LU-SGS. The Mach contour plots in Figure 10 show that KEPES-TeCNO gives much better shock resolution than KEPES, and comparable to the high-resolution Roe-MUSCL scheme.

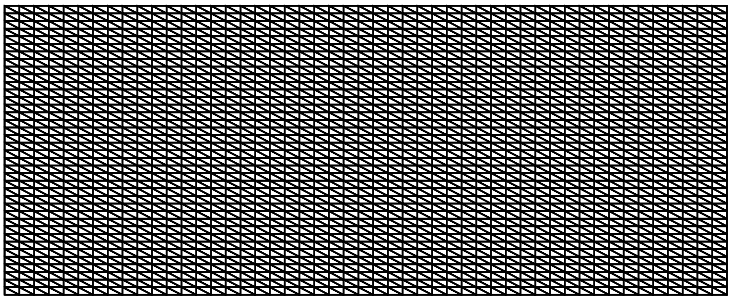

(a) Primal grid

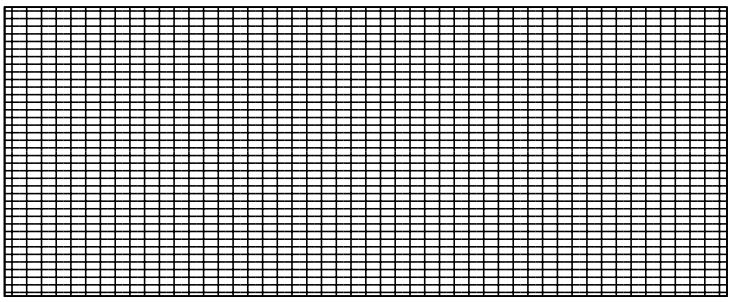

(b) Voronoi dual grid

Figure 5: Grid used for the shock tube problem

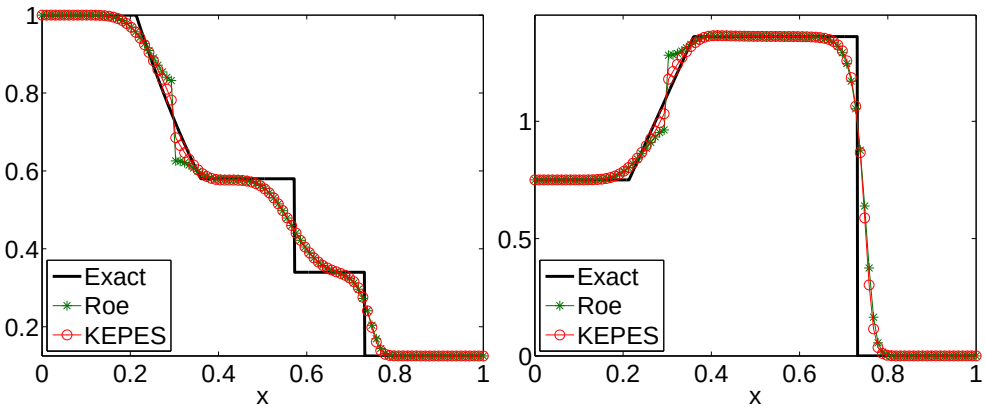

(a) Density (b) x-velocity

Figure 6: Modified shock tube problem using first order schemes

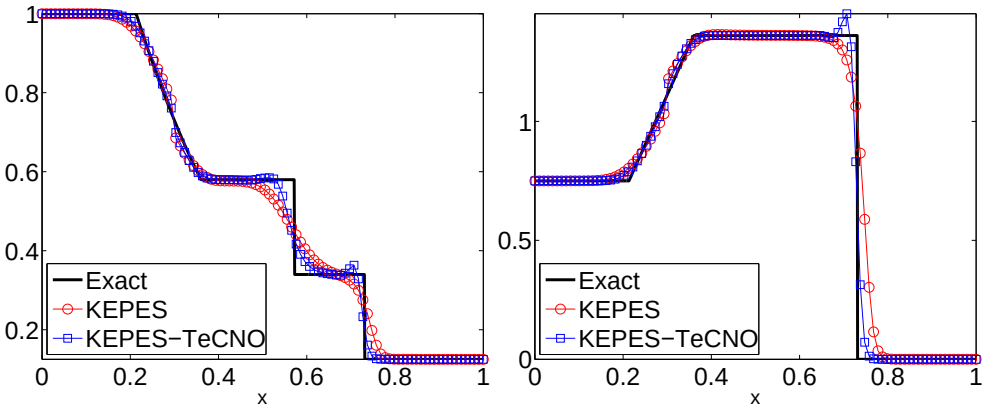

(a) Density (b) x-velocity

Figure 7: Comparison of KEPES and KEPES-TeCNO schemes

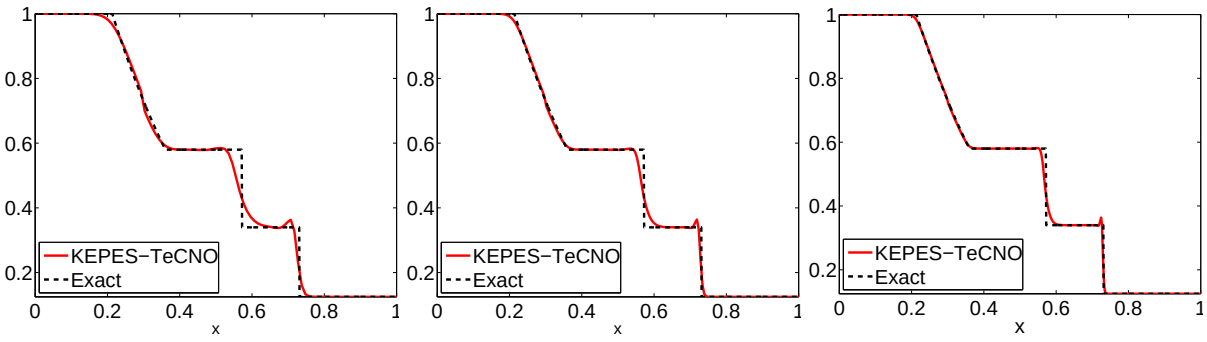

(a) $N = 100$ (b) $N = 200$ (c) $N = 400$

Figure 8: Density plot; grid refinement study with KEPES-TeCNO

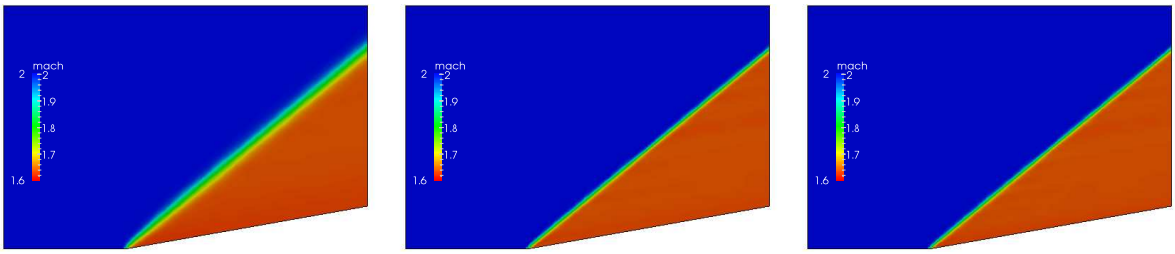

(a) KEPES (b) KEPES-TeCNO (c) Roe (MUSCL)

Figure 9: Mach number for supersonic flow over wedge

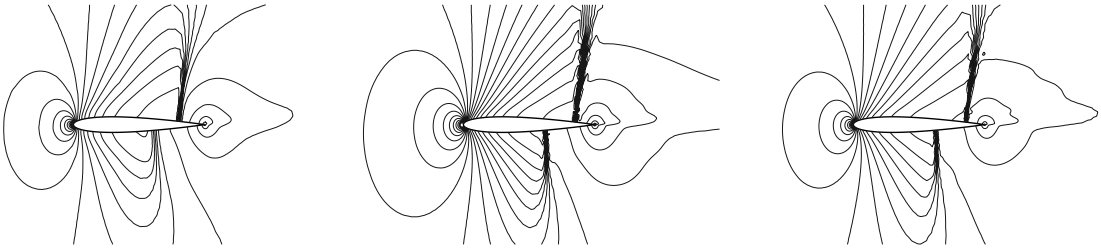

(a) KEPES (b) KEPES-TeCNO (c) Roe (MUSCL)

Figure 10: Mach number, 30 equally spaced contours between 0.04 and 1.7

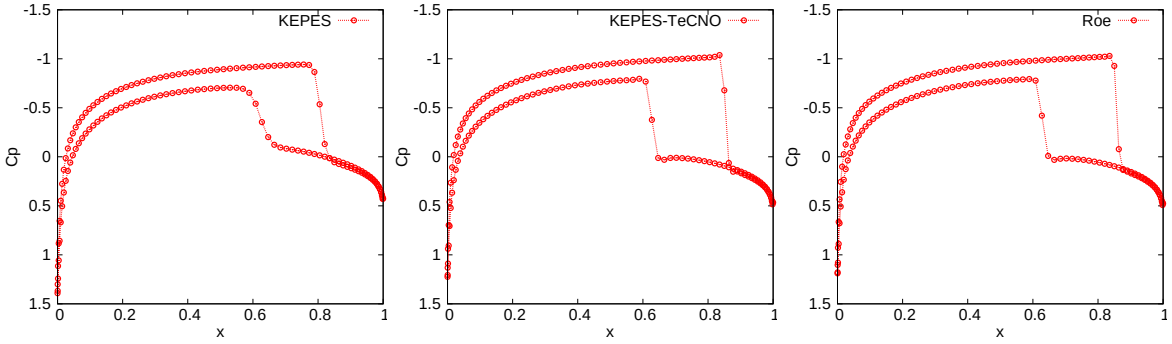

(a) KEPES (b) KEPES-TeCNO (c) Roe (MUSCL)

Figure 11: Pressure coefficient plots of the surface of the airfoil with $p_\infty = 0.9886$, $M_\infty = 0.85$

The pressure coefficient for compressible flows is given by

$$\mathrm{C}_p = \frac{2}{\gamma \mathrm{M}_\infty^2} \left(\frac{p}{p_\infty} - 1 \right)$$

where p is the nodal pressure, while p_∞ and M_∞ are the farfield pressure and Mach numbers respectively. We consider the nodal values of C_p on the surface of the airfoil, as shown in Figure 11. The x-axis represents the normalized wingspan, while the y-axis represents the inverted pressure coefficient. Thus, the upper surface of the wing, which has a much lower pressure distribution as compared to the lower surface, appears at the top of the plot. There is a sudden change in pressure across the shock that develops on both surfaces, and is clearly visible in the C_p plots. The area enclosed by the graph in the plots represents the lift experienced by the airfoil. Again, the high resolution KEPES-TeCNO was indistinguishable in accuracy with the standard high resolution Roe-MUSCL scheme.

4.4 Supersonic flow past cylinder

Most shock-capturing numerical schemes, except for a few highly dissipative schemes like the Rusanov scheme, can lead to numerical instabilities, particularly when approximating strong shocks. One of the most common anomalies is the *carbuncle phenomenon* [23, 24], which is produced when computing a supersonic flow past a blunt body such as a circular cylinder. Instead of having a smooth bow shock

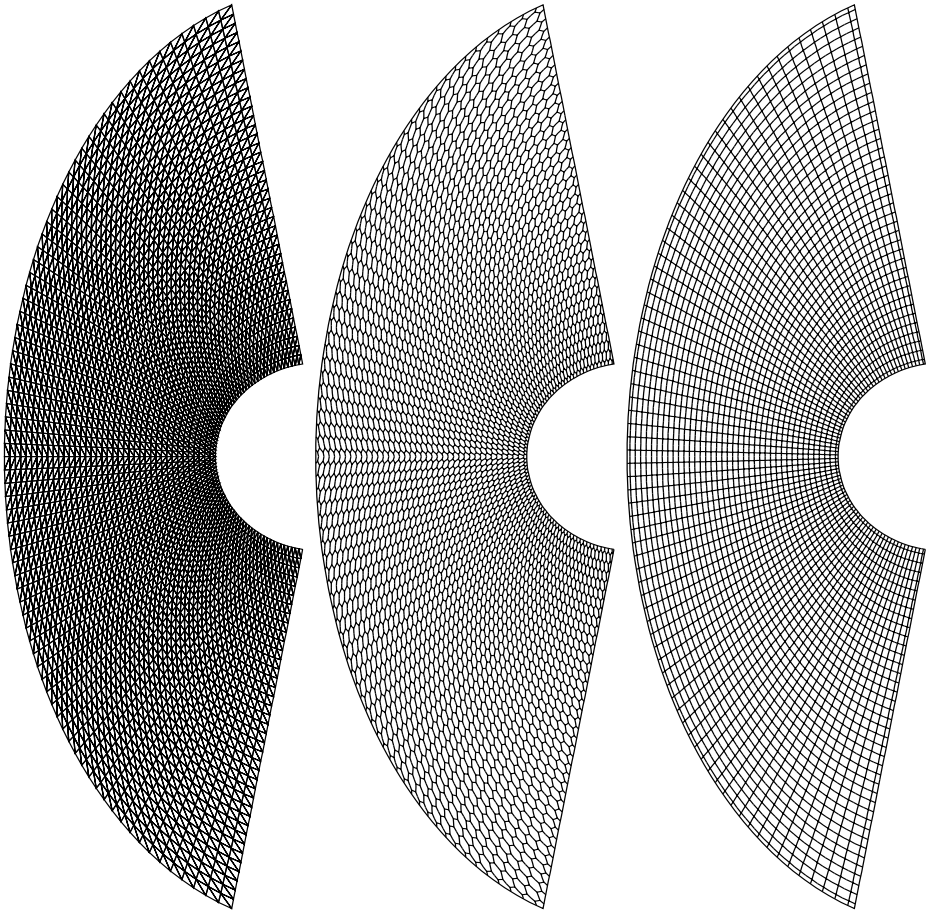

(a) Primal grid (b) Median dual grid (c) Voronoi dual grid

Figure 12: Grid used for supersonic cylinder problem

profile upstream of the cylinder, a protuberance appears ahead of the bow shock along the stagnation line. This effect seems to be more pronounced the more closely the grid is aligned to the bow shock.

Simulations were performed for the inviscid supersonic flow over a semi-cylinder. The primal triangular grid and the corresponding median and Voronoi dual meshes are shown in Figure 12. The Voronoi cells lead to nearly structured type grids and can thus lead to carbuncle problem since the shock will be aligned with the cell faces to a greater extent than for the median dual cells. At free-stream Mach number $M_\infty = 2$, KEPES and KEPES-TeCNO give carbuncle free solutions on both median dual and Voronoi dual meshes, as can be seen in Figure 13. The bow shock is well resolved in each case. Similar results were observed when the schemes were used to simulate an almost hypersonic flow with $M_\infty = 20$, as shown in Figure 14.

4.5 Subsonic flow past cylinder

We approximate the near incompressible limit of the Euler equations by considering an inviscid flow over a full cylinder at a low Mach number of 0.3. The steady state solution has both top-bottom and left-

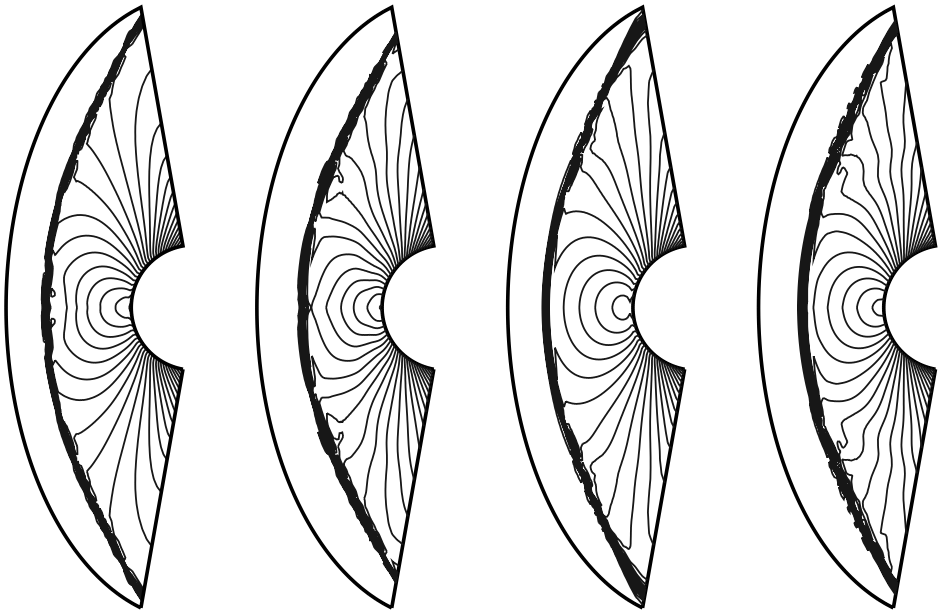

(a) KEPES (b) KEPES-TeCNO (c) KEPES (d) KEPES-TeCNO

Figure 13: Density contours for supersonic cylinder, $M_\infty = 2$. (a)-(b) median dual grid; (c)-(d) Voronoi dual grid

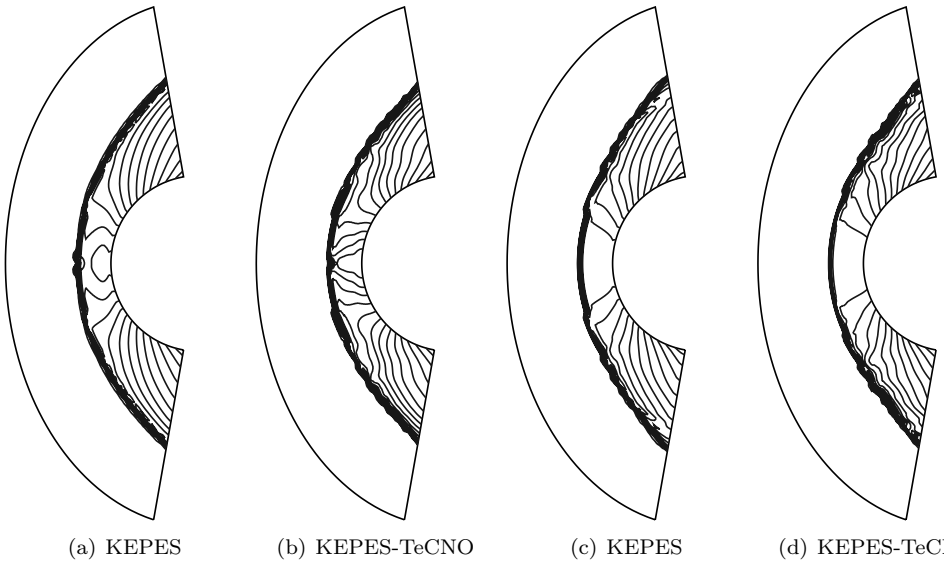

(a) KEPES (b) KEPES-TeCNO (c) KEPES (d) KEPES-TeCNO

Figure 14: Density contours for supersonic cylinder, $M_\infty = 20$. (a)-(b) median dual grid; (c)-(d) Voronoi dual grid

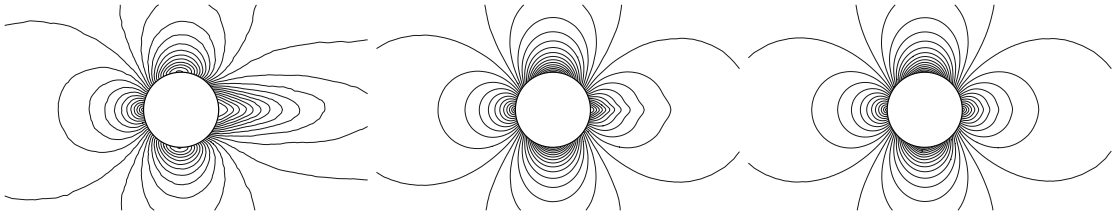

(a) KEPES (b) KEPES-TeCNO (c) KEPES2

Figure 15: Mach number, 30 equally spaced contours between 0.001 and 0.7

Scheme	**Minimum**	**Maximum**	**Percent deviation from s_∞**	
KEPES	2.07147	2.08695	+0.747 %	-0.000 %
KEPES-TeCNO	2.07147	2.07208	+0.029 %	-0.000 %
KEPES2	2.07139	2.07153	+0.003 %	-0.004 %

Table 1: Physical entropy bounds, with freestream $s_\infty = 2.07147$

right symmetry. The first order KEPES solution loses its symmetry due to the excessive dissipation, as shown in Figure 15. The KEPES-TeCNO does a much better job at preserving the symmetry property, comparable to the approximate solution given by the unlimited second order KEPES2 scheme.

The flow under consideration is nearly isentropic, that is, the physical entropy of the flow around the cylinder should be nearly constant. To demonstrate the ability of the schemes to preserve this constancy, the entropy bounds obtained with each scheme and their percentage deviation from the freestream entropy value are mentioned in Table 1. We notice that KEPES gives the largest positive deviation, KEPES2 gives almost negligible positive deviation, while the limited KEPES-TeCNO scheme lies somewhere in between. Both the entropy stable schemes show no negative deviations (as rigorously shown in this paper), while the KEPES2 scheme gives almost negligible negative deviation. Although the KEPES2 performs the best in this scenario, we cannot theoretically prove any stability estimates with it. Moreover, the unlimited KEPES2 would perform rather poorly in the presence of shocks.

4.6 Step in wind tunnel

This test case is described in [28] and involves an inviscid supersonic flow past a step in a wind tunnel which is impulsively started, with initial Mach number $M = 3$. The wind tunnel is one unit length wide and three unit lengths long. The step is 0.2 unit length high and is located 0.6 unit length from the left-hand end of the tunnel. At the left boundary, one imposes an inflow boundary condition. The exit boundary condition on the right has no effect on the flow, because the exit velocity is always supersonic. Along the top and bottom walls of the tunnel slip boundary conditions are applied. The corner of the step is the center of a rarefaction fan and hence is a singular point of the flow.

The flow develops several shocks which undergo further reflections. A shock triple point intersection leads to the formation of a slip line. The grid is adapted to be finer near the corner where the spacing is of size ≈ 0.002 while the maximum spacing is of size ≈ 0.01. The total number of gridpoints is 70970. The density contours at time $t = 4$ are shown in Figure 16 using the KEPEC-TeCNO scheme which is able to resolve the main features of the flow very accurately.

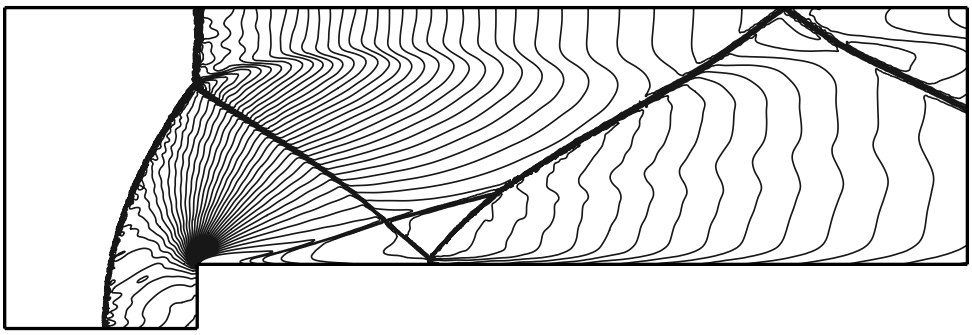

Figure 16: Density, 50 contour lines between 0.5 and 7.1 using KEPES-TeCNO at $t = 4$

5 Conclusions

We consider symmetrizable systems of conservation laws in two space dimensions and design a high-resolution *entropy stable* finite volume scheme to approximate them. The underlying computational domain is discretized using triangles and a finite volume scheme is proposed by combining entropy conservative fluxes and numerical dissipation operators, based on piecewise linear reconstruction that enforces a *sign property*. A minmod limiter, satisfying the sign property is used. The resulting scheme is

- Entropy stable i.e, satisfies a discrete form of the entropy inequality. Given that the underlying entropy is strictly convex, the discrete entropy inequality automatically guarantees a bound on the approximate solutions in L^2. To the best of our knowledge, the proposed KEPES-TeCNO scheme is one of the first high-resolution finite volume schemes that are shown (rigorously) to be entropy stable on unstructured grids.
- Robust in approximating complex flow features such as strong (supersonic) shocks, shock reflections, slip lines and near incompressible flows. The robustness of the scheme is demonstrated through a large number of benchmark numerical experiments that illustrate that the KEPES-TeCNO is at least as accurate as a standard high-resolution Roe-MUSCL method.

Thus, we design a scheme whose accuracy is at least comparable to existing high-resolution schemes but at the same time, the proposed scheme has rigorous stability properties. The numerical tests show that the scheme is able to preserve positivity of density and pressure without any additional treatment on unstructured grids. The current scheme is restricted to second-order resolution. Even higher-order schemes are currently being investigated. Future work will present the extension of the proposed methodology to the Navier-Stokes equations and to three space dimensions.

Acknowledgments This research work benefited from the support of the AIRBUS Group Corporate Foundation Chair in Mathematics of Complex Systems, established in TIFR/ICTS, Bangalore. The research of SM was partly supported by ERC StG NN. 306279 SPARCCLE.

Appendix A Roe-type dissipation for Euler equations

The Roe-type dissipation matrix is given by

$$\mathbf{D}_{ij} = \mathbf{R}_{ij}^{\top} \mathbf{\Lambda}_{ij} \mathbf{R}_{ij}$$

where

$$\mathbf{R} = \begin{pmatrix} 1 & 1 & 0 & 1 \\ u - a\tilde{n}_1 & u & \tilde{n}_2 & u + a\tilde{n}_1 \\ v - a\tilde{n}_2 & v & -\tilde{n}_1 & v + a\tilde{n}_2 \\ H - au_{\tilde{n}} & \frac{1}{2}|\mathbf{u}|^2 & u\tilde{n}_2 - v\tilde{n}_1 & H + au_{\tilde{n}} \end{pmatrix} \mathbf{S}^{\frac{1}{2}}$$

$$\mathbf{S} = \text{diag}\left(\tfrac{\rho}{2\gamma}, \quad \tfrac{(\gamma-1)\rho}{\gamma}, \quad p, \quad \tfrac{\rho}{2\gamma}\right)$$

$$\mathbf{\Lambda} = \text{diag}\left(|u_n - a|, \quad |u_n|, \quad |u_n|, \quad |u_n + a|\right).$$

In the above expressions, $\mathbf{S}$ is the scaling matrix for the eigenvectors, $\tilde{\mathbf{n}}$ is the unit outward normal on the faces, $u_{\tilde{n}} = \mathbf{u} \cdot \tilde{\mathbf{n}}$, $a = \sqrt{\frac{\gamma p}{\rho}}$ is the speed of sound in air and $H = \frac{a^2}{\gamma - 1} + \frac{|\mathbf{u}|^2}{2}$ is the specific enthalpy. The following average states are used to evaluate the above matrices:

$$\mathbf{u} = \overline{\mathbf{u}}_{ij}, \qquad \rho = \widehat{\rho}_{ij}, \qquad p = \frac{\overline{\rho}_{ij}}{2\overline{\beta}_{ij}}, \qquad a = \sqrt{\frac{\gamma}{2\widehat{\beta}_{ij}}}. \tag{A.1}$$

The KEPES scheme (see Section 4) is able to resolve stationary contact discontinuities exactly, if the speed of sound a in the dissipation operator $\mathbf{D}_{ij}$ is evaluated using the expression described in (A.1) [3].

References

[1] Timothy J. Barth. Numerical methods for gasdynamic systems on unstructured meshes. In *An introduction to recent developments in theory and numerics for conservation laws (Freiburg/Littenweiler, 1997)*, volume 5 of *Lect. Notes Comput. Sci. Eng.*, pages 195–285. Springer, Berlin, 1999.

[2] J. Blazek. *Computational Fluid Dynamics: Principles and Applications.* Elsevier Science, Oxford, second edition edition, 2005.

[3] Praveen Chandrashekar. Kinetic energy preserving and entropy stable finite volume schemes for compressible Euler and Navier-Stokes equations. *Commun. Comput. Phys.*, 14(5):1252–1286, 2013.

[4] Bernardo Cockburn and Chi-Wang Shu. TVB Runge-Kutta local projection discontinuous Galerkin finite element method for conservation laws. II. General framework. *Math. Comp.*, 52(186):411–435, 1989.

[5] Constantine M. Dafermos. *Hyperbolic conservation laws in continuum physics*, volume 325 of *Grundlehren der Mathematischen Wissenschaften [Fundamental Principles of Mathematical Sciences]*. Springer-Verlag, Berlin, third edition, 2010.

[6] J.-A. Désidéri and A. Dervieux. Compressible flow solvers using unstructured grids. In *Computational fluid dynamics, Vol. 1, 2*, volume 88 of *von Karman Inst. Fluid Dynam. Lecture Ser.*, page 115. von Karman Inst. Fluid Dynamics, Rhode-St-Genèse, 1988.

[7] U. S. Fjordholm, S. Mishra and E. Tadmor. Energy preserving and energy stable schemes for the shallow water equations. *"Foundations of Computational Mathematics"*, Proc. FoCM held in Hong Kong 2008 (F. Cucker, A. Pinkus and M. Todd, eds), London Math. Soc. Lecture Notes Ser. 363, pp. 93-139, 2009.

[8] U. Fjordholm, S. Mishra, and E. Tadmor. Arbitrarily high-order accurate entropy stable essentially nonoscillatory schemes for systems of conservation laws. *SIAM Journal on Numerical Analysis*, 50(2):544–573, 2012.

[9] U. S. Fjordholm. S. Mishra and E. Tadmor. ENO reconstruction and ENO interpolation are stable. *FoCM* 13 (2), 2013, 139–159.

[10] U. S. Fjordholm, R. Käppeli, S. Mishra and E. Tadmor. Construction of approximate entropy measure valued solutions for hyperbolic systems of conservation laws. *Preprint,* 2014, available from ArXiv 1402.0909.

[11] S. K. Godunov. An interesting class of quasilinear systems. *Dokl. Akad. Nauk. SSSR*, 139:521–523, 1961.

[12] Sigal Gottlieb, Chi-Wang Shu, and Eitan Tadmor. Strong stability-preserving high-order time discretization methods. *SIAM Rev.*, 43(1):89–112 (electronic), 2001.

[13] Amiram Harten. On the symmetric form of systems of conservation laws with entropy. *J. Comput. Phys.*, 49(1):151–164, 1983.

[14] T. J. R. Hughes, L. P. Franca, and M. Mallet. A new finite element formulation for computational fluid dynamics. I. Symmetric forms of the compressible Euler and Navier-Stokes equations and the second law of thermodynamics. *Comput. Methods Appl. Mech. Engrg.*, 54(2):223–234, 1986.

[15] Farzad Ismail and Philip L. Roe. Affordable, entropy-consistent euler flux functions ii: Entropy production at shocks. *Journal of Computational Physics*, 228(15):5410 – 5436, 2009.

[16] A. Jameson and D. Mavriplis. Finite volume solution of the two-dimensional Euler equations on a regular triangular mesh. *AIAA Journal*, 24:611–618, 1986.

[17] Antony Jameson. Formulation of kinetic energy preserving conservative schemes for gas dynamics and direct numerical simulation of one-dimensional viscous compressible flow in a shock tube using entropy and kinetic energy preserving schemes. *J. Sci. Comput.*, 34(2):188–208, 2008.

[18] D. Kröner, S. Noelle, and M. Rokyta. Convergence of higher order upwind finite volume schemes on unstructured grids for scalar conservation laws in several space dimensions. *Numerische Mathematik*, 71(4):527–560, 1995.

[19] D. Kröner and M. Rokyta. Convergence of Upwind Finite Volume Schemes for Scalar Conservation Laws in Two Dimensions. *SIAM Journal on Numerical Analysis*, 31(2):324–343, 1994.

[20] P. G. Lefloch, J. M. Mercier, and C. Rohde. Fully discrete, entropy conservative schemes of arbitrary order. *SIAM J. Numer. Anal.*, 40(5):1968–1992 (electronic), 2002.

[21] A. Madrane, Ulrik Fjordholm, Siddhartha Mishra, and Eitan Tadmor. Entropy conservative and entropy stable finite volume schemes for multi-dimensional conservation laws on unstructured meshes. Technical Report 2012-31, Seminar for Applied Mathematics, ETH Zürich, 2012.

[22] M. S. Mock. Systems of conservation laws of mixed type. *J. Differential Equations*, 37(1):70–88, 1980.

[23] J.-Ch. Robinet, J. Gressier, G. Casalis, and J.-M. Moschetta. Shock wave instability and the carbuncle phenomenon: same intrinsic origin? *J. Fluid Mech.*, 417:237–263, 2000.

[24] P. Roe, H. Nishikawa, F. Ismail, and L. Scalabrin. On carbuncles and other excrescences. In *17th AIAA Computational Fluid Dynamics Conference*, AIAA Paper 2005-4872, Toronto, 2005.

[25] P. L. Roe. Approximate Riemann solvers, parameter vectors, and difference schemes. *J. Comput. Phys.*, 43(2):357–372, 1981.

[26] E. Tadmor. Numerical Viscosity and the Entropy Condition for Conservative Difference Schemes. *Mathematics of Computation*, 43(168):pp. 369–381, 1984.

[27] Eitan Tadmor. Entropy stability theory for difference approximations of nonlinear conservation laws and related time-dependent problems. *Acta Numer.*, 12:451–512, 2003.

[28] Paul Woodward and Phillip Colella. The numerical simulation of two-dimensional fluid flow with strong shocks. *J. Comput. Phys.*, 54(1):115–173, 1984.

Recent Research Reports

Nr.	Authors/Title

2014-18 D. Conus and A. Jentzen and R. Kurniawan
Weak convergence rates of spectral Galerkin approximations for SPDEs with nonlinear diffusion coefficients

2014-19 J. Doelz and H. Harbrecht and Ch. Schwab
Covariance regularity and H-matrix approximation for rough random fields

2014-20 P. Grohs and S. Hosseini
Nonsmooth Trust Region Algorithms for Locally Lipschitz Functions on Riemannian Manifolds

2014-21 P. Grohs and A. Obermeier
Optimal Adaptive Ridgelet Schemes for Linear Transport Equations

2014-22 S. Mishra and Ch. Schwab and J. Sukys
Multi-Level Monte Carlo Finite Volume methods for uncertainty quantification of acoustic wave propagation in random heterogeneous layered medium

2014-23 J. Dick and Q. T. Le Gia and Ch. Schwab
Higher order Quasi Monte Carlo integration for holomorphic, parametric operator equations

2014-24 C. Sanchez-Linares and M. de la Asunci on and M. Castro and S. Mishra and J. Šukys
Multi-level Monte Carlo finite volume method for shallow water equations with uncertain parameters applied to landslides-generated tsunamis

2014-25 R.N. Gantner and Ch. Schwab
Computational Higher Order Quasi-Monte Carlo Integration

2014-26 C. Schillings and Ch. Schwab
Scaling Limits in Computational Bayesian Inversion

2014-27 R. Hiptmair and A. Paganini
Shape optimization by pursuing diffeomorphisms